Variations in Ground Motion Amplification in the Los Angeles Basin due to the 2019 M7.1 Ridgecrest Earthquake: Implications for the Long-Period Response of Infrastructure

Monica D. Kohler, Ph.D.,[1] Filippos Filippitzis, Ph.D.,[1] Robert Graves, Ph.D.,[2] Anthony Massari, Ph.D., P.E.,[3] Thomas Heaton, Ph.D.,[1] Robert Clayton, Ph.D.,[4] Julian Bunn, Ph.D.,[5] Richard Guy, Ph.D.,[4] and K. Mani Chandy, Ph.D. [6]

[1]Division of Engineering and Applied Science, Department of Mechanical and Civil Engineering, California Institute of Technology, Pasadena, CA 91125; email: kohler@caltech.edu
[2]U.S. Geological Survey, Pasadena, CA 91106
[3]Department of Engineering Civil, Environmental and Geodetic Engineering, The Ohio State University, Columbus, OH, 43210
[4]Division of Geological and Planetary Sciences, Seismological Laboratory, California Institute of Technology, Pasadena, CA 91125
[5]Division of Physics, Math and Astronomy, Center for Data-Driven Discovery, California Institute of Technology, Pasadena, CA 91125
[6]Division of Engineering and Applied Science, Department of Computing and Mathematical Sciences, California Institute of Technology, Pasadena, CA 91125

ABSTRACT

Coherent patterns and large variations in ground shaking amplification were observed in the Los Angeles basin during the 2019 M7.1 Ridgecrest earthquake. In particular, 3 s to 6 s responses showed variations due to shallow basin geological structure that have implications for the response to large earthquakes of mid-rises, high-rises, long-span bridges, and fuel storage tanks, even if epicentral distances are several hundred kilometers. The Ridgecrest strong-motion data were recorded by seismic stations from the spatially dense Community Seismic Network, the Southern California Seismic Network, and the California Strong Motion Instrumentation Program. The mainshock observations are compared at the same locations with ground motion simulations to examine the regions that experienced the largest shaking, and to investigate the geological sources of large-amplitude shaking. The simulations were computed for the two most commonly-used regional community seismic velocity models, CVM-S4.26.M01 ('CVM-S') and CVM-H 15.1.0 ('CVM-H'). Both observations and simulations are used in dynamic analysis with a finite-element model of an existing high-rise with ~6-second fundamental horizontal periods, located in downtown Los Angeles. The geographical variation in maximum story drift, story-level shear force, and story-level moment values suggest that the excitation of a

hypothetical high-rise located in an area characterized by the largest 6-s PSA values could be significantly larger than in a downtown Los Angeles location. Ground motion simulations using the CVM-H velocity model more closely predict the long-period site amplifications in greater Los Angeles, particularly in the south-central San Fernando Valley, than simulations using CVM-S.

INTRODUCTION

The M7.1 Ridgecrest earthquake added to a growing list of large-magnitude California earthquakes that have produced amplified long-period ground shaking in greater Los Angeles, even when epicentral distances are large (~200+ km). A pattern of geographical distribution of long-period amplification is present for the largest (magnitude > 7) southern California earthquakes that have occurred since the advent of modern, dense, seismic instrumentation. Specifically, the 1992 Mw7.3 Landers, the 1999 Mw7.1 Hector Mine, and the 2010 Mw7.2 El Mayor-Cucapah earthquakes showed large long-period motions in the Los Angeles basin (Wald and Graves, 1998; Grazier et al., 2002; Hatayama and Kalkan, 2011), with associated distances of ~170 km for Landers, ~190 km for Hector Mine, and ~340 km for El Mayor-Cucapah (Fig. 1). For the more recent and more densely recorded 2010 El-Mayor-Cucapah earthquake, Hatayama and Kalkan (2011) found multiple zones of strong amplification in the Los Angeles basin, with the largest values occurring in a region in the western margin of the central Los Angeles basin, from analysis of long-period ($\geqslant$ 4 s) Fourier spectra relative to bedrock stations.

Recent studies of peak ground motions and pseudo-spectral accelerations in the Los Angeles basin from the 2019 M7.1 Ridgecrest earthquake illustrate how spatially coherent behavior occurs for periods $\geqslant$ 3 s, and that the maximum site amplification factor is 10 for 6 s (Kohler et al. 2020; Filippitzis et al. 2021). These findings were computed from the ratio of response spectral values combined for the two orthogonal horizontal directions, and are relative to the average of three bedrock sites in the Santa Monica Mountains, the San Rafael Hills, and the San Gabriel Mountains. Specifically, for long periods, the maximum peak ground motions and site amplifications were found in the western part of the Los Angeles basin and in the south-central San Fernando Valley sedimentary basin. The strong-motion data used by Kohler et al. (2020) and Filippitzis et al. (2021) came from the Southern California Seismic Network (SCSN), the California Strong Motion Instrumentation Program (CSMIP), and the Community Seismic Network (CSN).

In this study, rather than comparing observed vs. simulated ground motions and their spatial variations, we investigate several engineering parameters − inter-story drift, story-level shears and story-level moments − for a common high-rise structure type with long resonant periods. One goal is to examine the geographical variations in predicted maximum drifts, shear forces, and moments, and to compare these values for observed and simulated time histories from the 2019 Ridgecrest earthquake response in urban Los Angeles. A second goal is to map out regions that experienced the largest of these values in order to make a prediction for future

long-period response that may occur for large-magnitude earthquakes. We used the observed and simulated Ridgecrest ground motions in linear dynamic analysis with a finite-element model already developed and validated for an existing 52-story high-rise located in downtown Los Angeles. In our analysis, we computed inter-story drift, story-level shear forces, and story-level moments using this model, where maxima in these values are measures of building damage potential. The geographical variation in these values were compared with the response spectra results described in Kohler et al. (2020) and Filippitzis et al. (2021) to investigate how well the response spectra predicted building deformation, considering both observations and simulations.

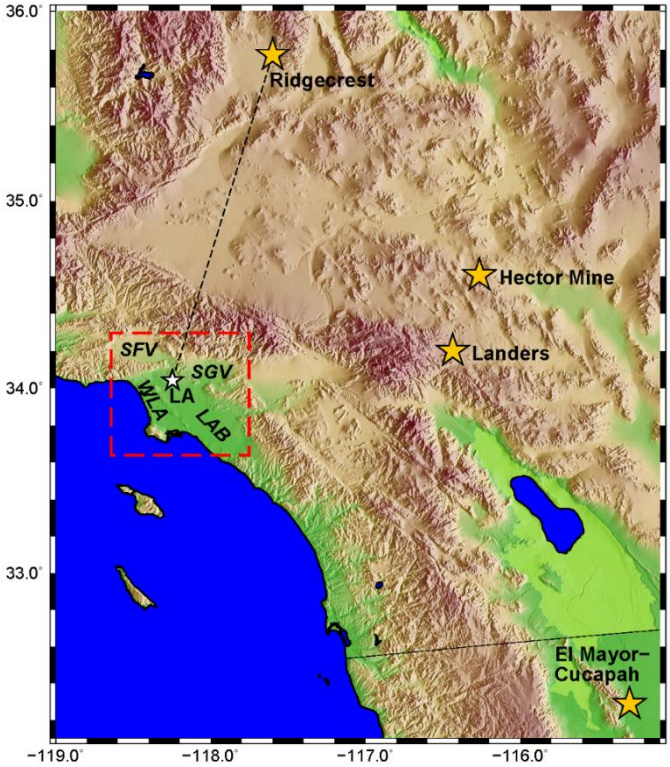

Figure 1. Topographic map of Southern California. Yellow stars show epicenters of 1992 M7.3 Landers, 1999 M7.1 Hector Mine, 2010 M7.2 El Mayor-Cucapah and 2019 M7.1 Ridgecrest earthquakes. Red dashed box shows focus area of Ridgecrest study. Black dashed line shows shortest source-to-receiver path between 2019 M7.1 Ridgecrest epicenter and Los Angeles. LA=Los Angeles. WLA=West Los Angeles, SFV=San Fernando Valley, LAB=Los Angeles Basin, SGV=San Gabriel Valley.

GROUND MOTION SIMULATION METHOD

The ground motion simulations for the 2019 M7.1 Ridgecrest earthquake were computed with the Graves (1996) 3D finite-difference method, which uses the Graves and Pitarka (2020) stochastic finite-fault rupture method. The rupture model uses the Graves and Pitarka (2016) kinematic rupture generator method and is constrained by near-fault ground motion observations.

The simulations use a minimum shear-wave velocity of 500 m/s and 100 m grid spacing, resulting in velocity ground motions with energy content containing frequencies up to 1 Hz. Anelastic attenuation Q_S is defined by $Q_S = 50V_S$ where V_S is shear-wave velocity in km/s, and is related to damping d, by d=1/2Q_S.

The simulations were carried out using 3D seismic velocity models CVM-H15.10.0 (Shaw et al., 2015) (hereafter referred to as 'CVM-H') and CVM-S4.26.M01 (Lee et al., 2014) (hereafter referred to as 'CVM-S'). Although both models cover approximately the same region and depth range, there are fundamental differences in the types of data that constrain parts of the models, particularly in the Los Angeles sedimentary basin ('LAB' in Fig. 1). Fig. 2 compares the results for 6-s pseudo-spectral accelerations (PSA) using 2% damping for the M7.1 Ridgecrest earthquake using the method described in Filippitzis et al. (2021). This figure illustrates the geospatial variation in the PSA values computed for data (Fig. 2a) and synthetic ground motions computed using CVM-H (Fig. 2b) and CVM-S (Fig. 2c).

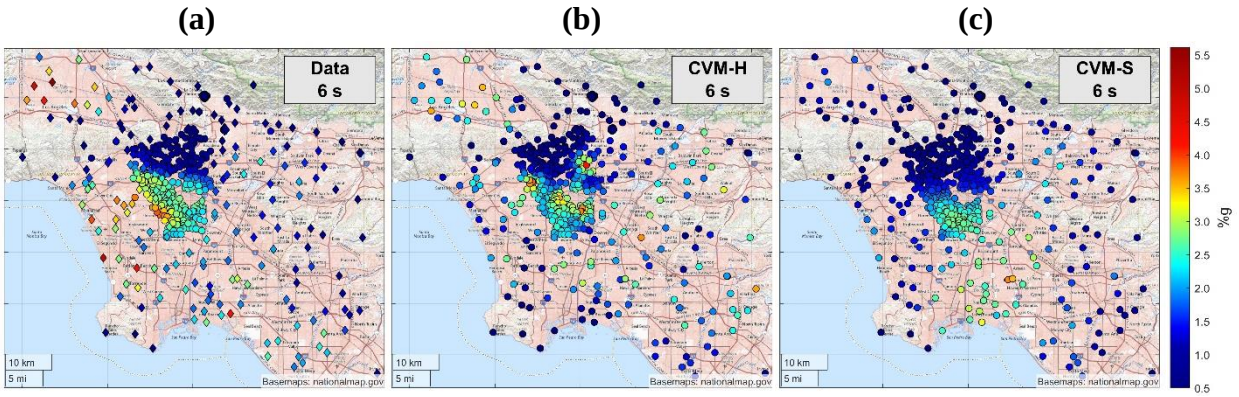

Figure 2. Geospatial variations in 6-s PSA values with 2% damping using M7.1 Ridgecrest accelerations for: a) Data; b) CVM-H simulations; c) CVM-S simulations. PSA amplitude scales are identical. Analysis is from Filippitzis et al. (2021).

HIGH-RISE DYNAMIC ANALYSIS METHOD

The high-rise finite-element model is based on an existing 52-story (+ 5 basement levels) dual steel moment and braced frame system building located in Los Angeles. This building's lateral system consists of a braced frame core surrounded by a steel moment frame. The floor plans contain various setbacks and notches along the building's vertical profile. The structural system consists of three major components: an interior concentrically braced core, outrigger beams spanning the core to the building perimeter, and eight exterior outrigger columns. The beams support gravity loads, act as ductile moment-resisting beams between the core and exterior frame columns, and enhance the overturning resistance of the building by engaging the perimeter columns to the core columns (Taranath, 1997). The first two translational resonant periods of this building in the horizontal directions are approximately 5.7 s and 1.7 s (Kohler et al., 2016). In

dual lateral systems such as this, the overall story stiffness is controlled by the interplay between the moment frames and the braced frames, whose properties vary vertically. At the bottom of the building, the stiffness contribution from the moment frames relative to the braced frames is larger than at the top, resulting in vertical variations in relative story-level shear and story-level moment. These in turn will contribute complexity to the maximum inter-story drift values when comparing location to location.

The computations described below are carried out with a linear finite-element model of the building which was developed based on detailed information obtained from a complete set of structural drawings. The major structural and connection elements obtained from the drawings are modeled using object-based physical-member modeling, such as built-in steel sections and braces (ETABS, Computers and Structures, Inc.). More details on the model construction and validation with local earthquake data are described in Kohler et al. (2016). Here we focus on linear elastic dynamics for the recorded acceleration time series from observed and simulated M7.1 Ridgecrest data for 20 seismic stations in the Los Angeles basin that had the largest recorded 6-s PSA values (Table 1). The linear-elastic dynamic response to the earthquake acceleration inputs in the EW and NS directions are computed using the ETABS model. A broadband Butterworth filter is applied to the observations and simulation results for frequencies between 0.1 and 25 Hz. The response is modeled in a fixed-base coordinate system.

RESULTS

We compute commonly-used engineering parameters in order to examine the geographical variations in their values for the largest of the observed long-period M7.1 Ridgecrest datasets, and for their associated simulated accelerations. In addition, we examine the vertical variations in these values within the building for complexity from multi-modal contributions. We focused on the 20 seismic stations that produced the largest 6-s PSA values for the high-rise dynamic analysis. The goal was to show how well the maxima in predicted (i.e. computed) drifts, story-level shear and story-level moments for a high-rise would compare in station locations with the largest 6-s PSA values. These 20 stations consisted of SCSN, CSMIP and CSN stations, mostly located in West Los Angeles and the south-central San Fernando Valley (Table 1).

Fig. 3a shows the maximum building-EW component inter-story drift results of the linear analysis for the high-rise, using M7.1 Ridgecrest recorded data as time history input into the ETABS model. The curves show the maximum values for each floor, independent of the time at which the maximum occurred; thus they are not all from the same instance of time. All 20 station inputs resulted in parameters that are well within the linear regime; however, while most values are small, one station (CE.24805 in Northridge, CA) resulted in significantly larger parameters than the rest, and primarily in the building-EW direction. Fig. 3b shows the analogous results for seismic velocity model CVM-H, and Fig. 3c shows the results for CVM-S. The CVM-H simulations also predict the largest inter-story drift values for a location in the San Fernando Valley (CE. Q0057 in Van Nuys, CA); however, Figs. 3b and 3c indicate that the simulations,

particularly those that use CVM-S, significantly underpredict the long-period ground motions in general in both the San Fernando Valley and West Los Angeles.

Table 1. Seismic stations in greater Los Angeles with maximum 6-second PSA values from the M7.1 2109 Ridgecrest earthquake. PSA=pseudo-spectral acceleration for 6 seconds with 2% damping. PGA=Peak ground acceleration. Network codes: CE=CSMIP, CI=Southern California Seismic Network, CJ=Community Seismic Network.

Station name	Net-work	Station location	Station coordinates	PGA (%g)	6-sec PSA (%g)
24805	CE	Northridge, CA	34.2289 -118.5289	4.31	5.61
14221	CE	Manhattan Beach, CA	33.8883 -118.4098	1.49	4.97
24806	CE	Winnetka, CA	34.2218 -118.5714	2.83	4.61
LAF	CI	Torrance, CA	33.8689 -118.3314	1.22	4.30
24866	CE	Reseda, CA	34.1934 -118.5484	3.25	4.14
PDR	CI	Playa Del Rey, CA	33.9627 -118.4370	1.54	3.92
T001227	CJ	Southcentral Los Angeles, CA	33.9773 -118.2843	2.07	3.88
T001213	CJ	Southcentral Los Angeles, CA	33.9713 -118.2761	2.01	3.82
T000887	CJ	View Park-Windsor Hills, CA	34.0059 -118.3357	2.25	3.77
Q0057	CI	Van Nuys, CA	34.1876 -118.4771	3.45	3.77
T001211	CJ	Southcentral Los Angeles, CA	33.9776 -118.2758	2.24	3.74
T001214	CJ	Southcentral Los Angeles, CA	33.9696 -118.2670	2.53	3.74
LCG	CI	Ladera Heights, CA	34.0003 -118.3779	1.81	3.73
24013	CE	Canoga Park, CA	34.1941 -118.5888	2.43	3.59
BHP	CI	View Park-Windsor Hills, CA	33.9905 -118.3617	1.51	3.58
T001228	CJ	Southcentral Los Angeles, CA	33.9862 -118.2939	2.06	3.58
T001229	CJ	Southcentral Los Angeles, CA	33.9858 -118.2884	1.94	3.57
T001215	CJ	Southcentral Los Angeles, CA	33.9680 -118.2604	1.64	3.56
T001212	CJ	Southcentral Los Angeles, CA	33.9796 -118.2680	1.93	3.49
14820	CE	View Park-Windsor Hills, CA	33.9934 -118.3425	1.99	3.47

Figs. 3abc show several vertical profile curves (i.e. different seismic stations) that cross over each other as a function of building height. This may indicate the impact of lowest-frequency vs. higher-frequency modal contributions to the relative displacements within the building. The building-NS component results for all three datasets are smaller-amplitude, and show similar geographical variation across seismic stations, as well as similar relative amplitudes between observed data and simulations. As with the EW results, the NS drift curves also show some cross-over, indicating low-frequency vs. higher-frequency modal contributions to the NS relative displacements that are dependent on the frequency content of the time history input.

The results for maximum EW story-level shear force and moment values can be seen in Figs. 4 and 5, and as before are not all from the same time instance. The shear forces are computed by ETABS using constitutive relations determined by the structural elements making up the model, together with the computed deflections, integrated at every story along each direction of interest. Here, we refer to the EW moments as those that are caused by forces

applied in the EW direction. Figs. 4a and 5a show the story-level shear and moment results of the linear analysis for the high-rise using the M7.1 Ridgecrest recorded data as input. Figs. 4b and 5b show the analogous results for seismic velocity model CVM-H, and Figs. 4c and 5c show the results for CVM-S. As with inter-story drift analysis, the CVM-H simulations predict the largest story-level shear and moment values for station CE.Q0057 located in Van Nuys, CA; however, the simulations also significantly underpredict the overall story-level shear and moment values for all 20 locations. As with drift, Figs. 4abc also show several vertical profile curves that cross

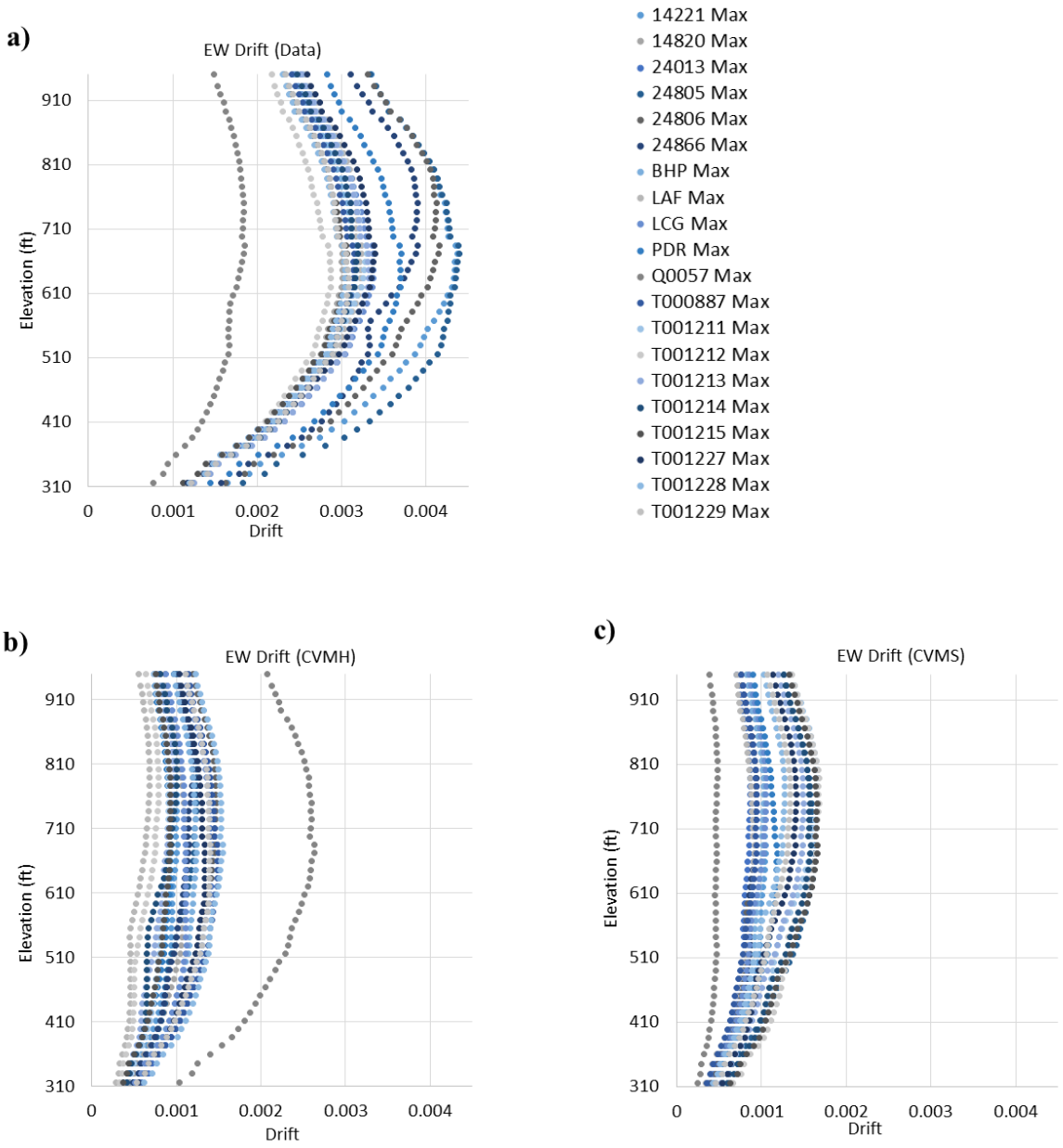

Figure 3. Maximum EW inter-story drift computations using finite-element model of high-rise with M7.1 Ridgecrest time histories from: a) Data; b) CVM-H simulations; c) CVM-S simulations. Horizontal amplitude scales are identical. Station locations are shown in Table 1.

over others, vertically within the building, indicating the varying contributions of the lowest-frequency vs. higher-frequency modes to the shear force distribution. The NS-component results for all three datasets show similar geographical variation across seismic stations, as well as similar relative amplitudes between observed data and simulations.

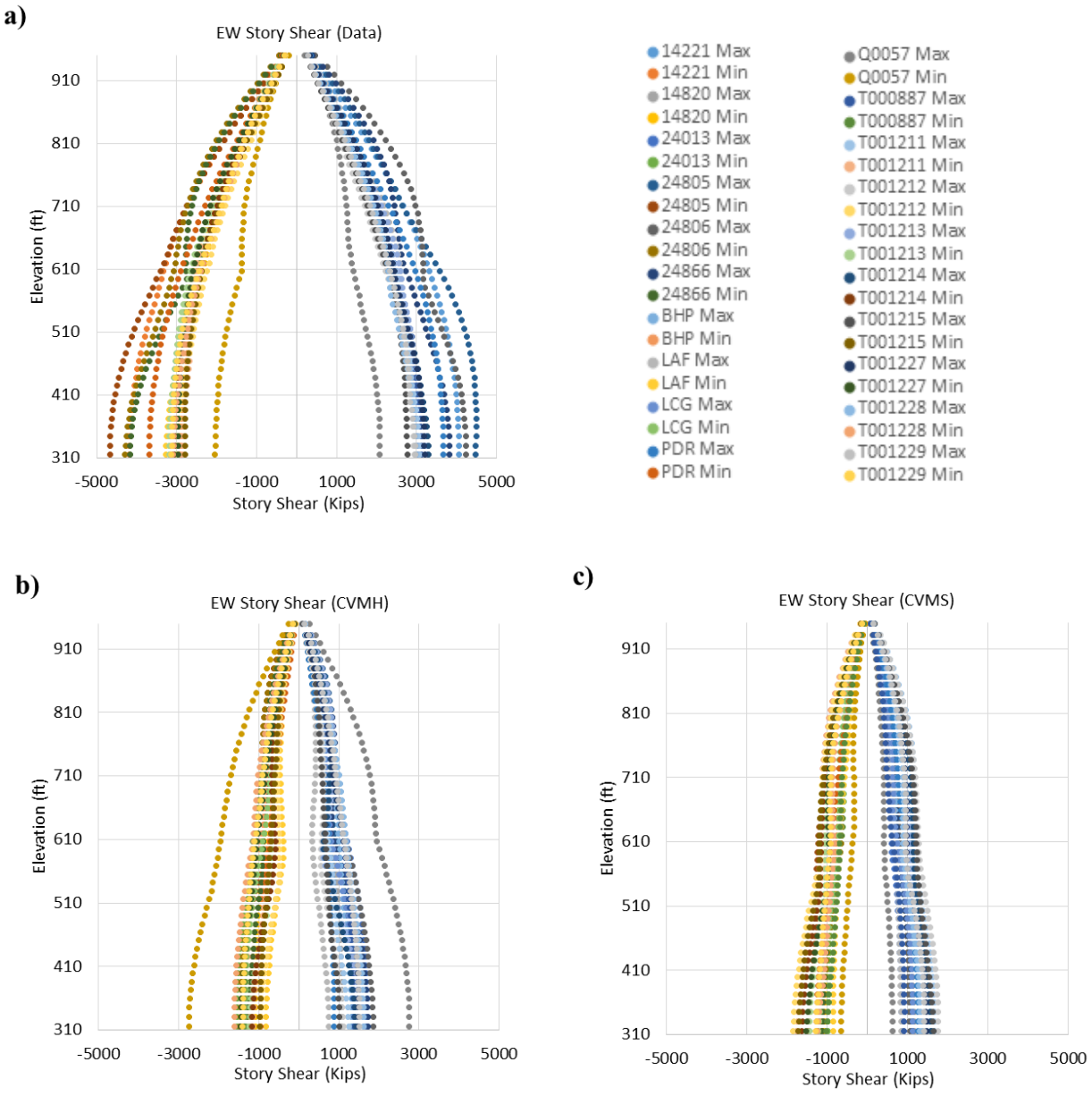

Figure 4. Maximum EW story-level shear computations using finite-element model of high-rise with M7.1 Ridgecrest time histories from: a) Data; b) CVM-H simulations; c) CVM-S simulations. Horizontal amplitude scales are identical. Station locations are shown in Table 1.

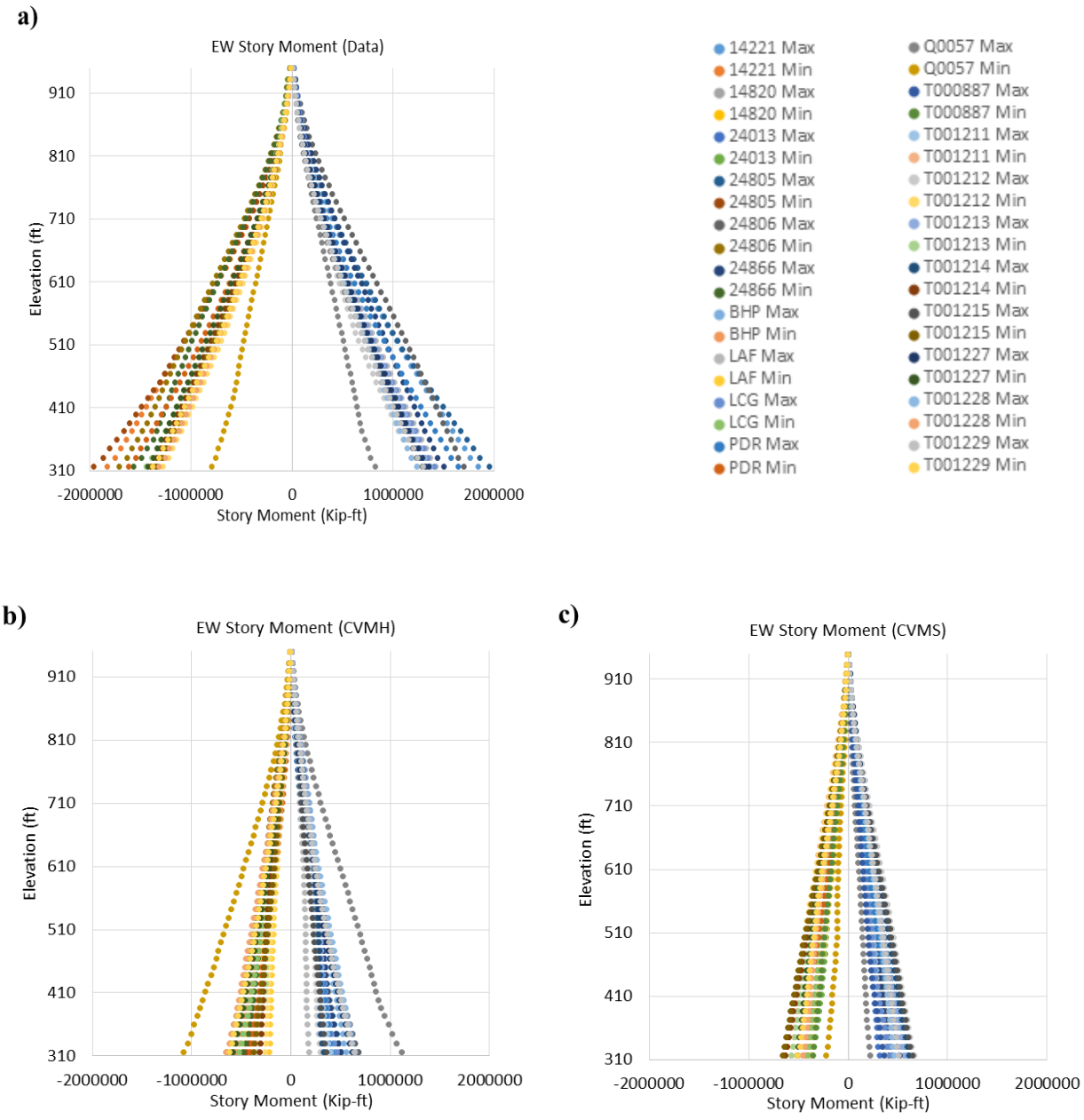

Figure 5. Maximum EW story-level moment computations using finite-element model of high-rise with M7.1 Ridgecrest time histories from: a) Data; b) CVM-H simulations; c) CVM-S simulations. Horizontal amplitude scales are identical. Station locations are in Table 1.

The geospatial variations in maximum values for drift, and story-level shear forces and moments are shown in Figs. 6-8 for the 20 stations listed in Table 1. Figs. 6a, 7a and 8a show the variations in values for the observed data. Figs. 6b, 7b, and 8b and Figs. 6c, 7c, and 8c show the variations for the simulation inputs using CVM-H and CVM-S respectively. The smaller gray

dots in these figures show the other stations used in Filippitzis et al. (2021), but which had smaller 6-s PSA values.

Figs. 6-8 illustrate the consequences of the differences between the two velocity models and their consequential effects on ground motion computations. The result is that the larger, long-period motions in the central San Fernando Valley (Figs. 2, 6-8) are better predicted with CVM-H than with CVM-S, possibly due to the additional data constraints on the uppermost crustal velocities (at depths of < 6 km). In addition, as Fig. 2 shows, both simulation sets predict larger motions within the central Los Angeles basin where the basin depth is approx. 9 km, but the locations of the largest motions do not agree with the data. The amplitudes and geographical locations of the largest long-period ground motions suggest that the source of discrepancy between simulations and data is more likely to be due to incomplete or inaccurate velocity model near the receivers than misrepresentation of the source rupture. Both velocity models contain a geotechnical layer that is based primarily on Vs30 values (Thompson, 2018) but is implemented differently in each. In these velocity models, the shallow near-surface basin velocities may not accurately capture the true low-velocity soil layers which can be much lower than 500 m/s. However, the low-velocity layers are thin relative to the wavelengths and depth sensitivity kernels associated with the seismic waves examined here, and should not have a significant impact on the > 1 s periods that predominate the high-rise's long-period response and the ground motion simulation time histories. In CVM-H, the general basin depths are constrained by inclusion of gravity data, and basin geometries have sharper definition compared to CVM-S. The structural representation of CVM-H honors the major faults from the SCEC Community Fault Model, including within sedimentary basins such as the Los Angeles basin. As a result, the model contains lateral, fault-defined discontinuities that can affect wave propagation paths and velocities. Velocities within basins in CVM-H are determined from oil company reflection/refraction surveys and borehole profiles. The geotechnical layer (upper 350 m) tapers to Wills et al. (2015) Vs30 values at the surface, and velocities outside basins are updated using waveform tomography for periods ≥ 5 s. In CVM-S, basin depths are also constrained by inclusion of gravity data in CVM-S. The original velocities within the basins are from depths and ages of geological horizons calibrated to available sonic logs. The geotechnical layer (upper 350 m) is based on surface geology (rock or soil) and interpolation of selected vertical profiles. Velocities throughout the model are updated using waveform tomography for periods ≥ 5 s; thus, below about 6 km depth, crustal velocities of both models are similar.

CONCLUSIONS

The high-resolution recordings of the M7.1 Ridgecrest earthquake revealed variations in long-period ground motions on small spatial scales that was made possible by long-term continuous earthquake monitoring by seismic networks. Ground motion simulations for the 20 largest-amplitude recordings of long-period motion in greater Los Angeles indicate that ground

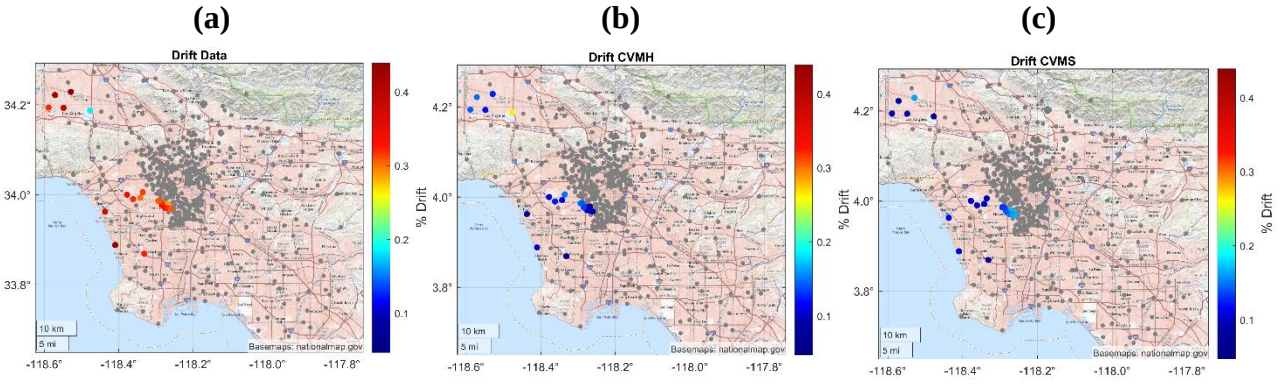

Figure 6. Geospatial variations in maximum values of EW inter-story drift computed from finite-element model using M7.1 Ridgecrest time histories for: a) Data; b) CVM-H simulations; c) CVM-S simulations. Drift amplitude scales are identical.

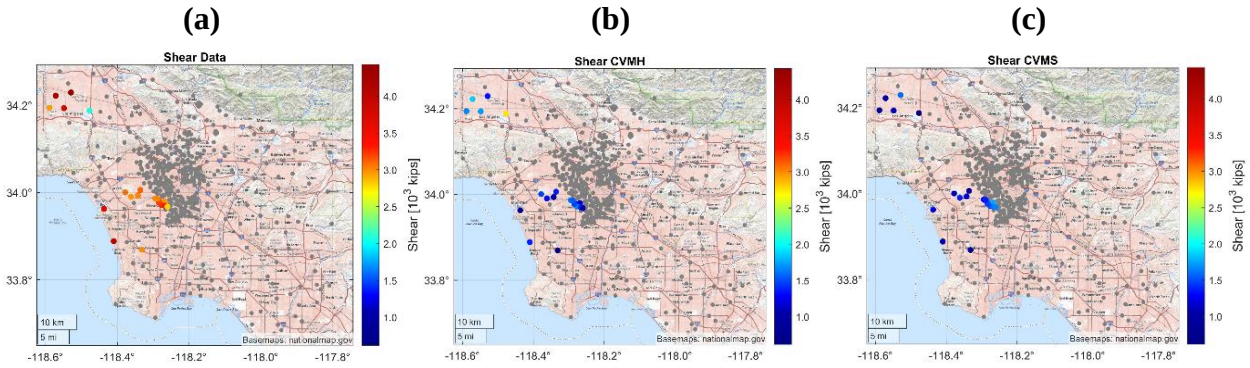

Figure 7. Geospatial variations in maximum values of EW story-level shear force computed from finite-element model using M7.1 Ridgecrest time histories for: a) Data, b) CVM-H simulations, c) CVM-S simulations. Shear force amplitude scales are identical.

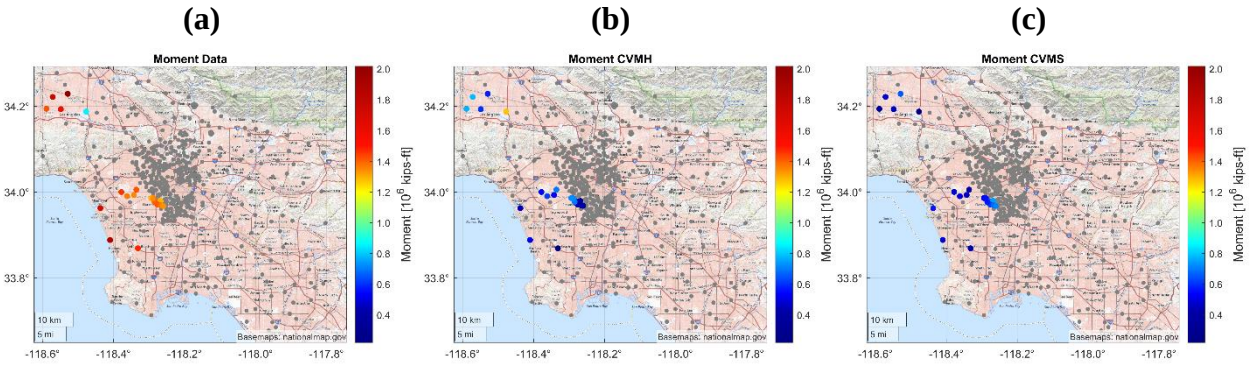

Figure 8. Geospatial variations in maximum values of EW story-level moment computed from finite-element model using M7.1 Ridgecrest time histories for: a) Data; b) CVM-H simulations; c) CVM-S simulations. Moment amplitude scales are identical.

motions are better estimated using the seismic velocity model CVM-H whose upper crustal velocity discontinuities are constrained by fault locations. However, both CVM-H and CVM-S models underpredict the long-period PSAs observed in the San Fernando Valley and in West Los Angeles. Linear dynamic analysis with a finite-element model based on an existing 52-story building located in downtown Los Angeles shows similar variations in predictions of drift, shear forces, and moments as a function of geographical location. The ground motion and high-rise engineering parameter assessments presented here have implications for future new engineering developments that include high-rise, mid-rise and low-rise structures and associated infrastructure, such as that planned for the western San Fernando Valley (Los Angeles Times, 2020). The results support the denser (~1 km) deployment of a larger number of permanent seismic stations in order to record large-magnitude earthquakes for use in future updates of the seismic velocity models for applications such as deterministic seismic hazard analysis.

While both velocity models have incorporated a large number of different data sources, they may both benefit from crustal velocity interfaces that are better-constrained by lithology and chronostratigraphy units, for example those provided by Ponti and Martin (2021). That study uses downhole lithologic and geophysical logs collected at water well sites. NMR, resistivity, reflection data, and oil and water well log data are combined to map the time-based stratigraphy of shallow crustal units below greater Los Angeles for use in hydrologic modeling. One result of the high-resolution data aggregation in Ponti and Martin (2021) is the 3D mapping of chronostratigraphic units from the surface to a depth of >10 km. These units indicate the locations and geometries of aquifer-related basins, and the bottom boundary defining the basin-bedrock interface. Moreover, the mapping shows the lateral extent of coarse-grained and fine-grained materials, which in turn may affect the seismic velocities and amplitudes of through-going waves. The mapping study suggests how the geotechnical layer can be expanded so that it is not just a near-surface layer (currently, implementation is in the uppermost 300-350 m). The geotechnical layer could be connected with structures in the upper 1-2 km, for example with structures described in Ponti and Martin (2021), which would help in the modeling of longer (and shorter) period motions. Mapped units such as those constrained by numerous water well log datasets indicate that the Los Angeles basin is more accurately defined by a series of sub-parallel troughs rather than a single long basin. The added complexity of multiple troughs has significant implications for how the effects of basin depth and edges should be accounted for in predictions of future ground motions.

ACKNOWLEDGMENTS

We are grateful to Caltech, the Betty and Gordon Moore Foundation, the Conrad N. Hilton Foundation, and Computers & Structures, Inc., for providing support for the Community Seismic Network and for this study.

REFERENCES

ETABS, Structural and Earthquake Engineering Software, Computers and Structures, Inc., Berkeley, CA, www.csi.berkeley.com, 1995. http://docs.csiamerica.com/manuals/etabs/Analysis%20Reference.pdf.

Filippitzis, F., Kohler, M. D., Heaton, T. H., Graves, R. W., Clayton, R. W., Guy, R. G., Bunn, J. J., Chandy, K. M. (2021). "Ground motions in urban Los Angeles from the 2019 Ridgecrest earthquake sequence." *Earthquake Spectra*, early version available online, doi:10.1177/87552930211003916.

Graves, R. W. (1996). "Simulating seismic wave propagation in 3D elastic media using staggered-grid finite differences." *Bull. Seis. Soc. Am*., 86(4), pp.1091-1106.

Graves, R. W. and Pitarka, A. (2016). "Kinematic ground-motion simulations on rough faults including effects of 3D stochastic velocity perturbations." *Bull. Seis. Soc. Am*., 106(5), 2136-2153.

Graves, R. W. and Pitarka, A. (2020). "3D Ground Motion Simulations for Events in the 2019 Ridgecrest Sequence." *17th World Conference on Earthquake Engineering, 17WCEE*, Sendai, Japan - September 13-18, 2020.

Grazier, V., Shakal, A., Scrivner, C., Hauksson, E., Polet, J., Jones, L. (2002). "TriNet strong-motion data from the M 7.1 Hector Mine, California Earthquake of 16 October 1999, *Bull Seis. Soc. Am*., 92(4), 1525-1542.

Hatayama, K., and Kalkan, E. (2011). "Long-period (3 to 10 s) ground motions in and around the Los Angeles basin during the M 7.2 El Mayor-Cucapah Earthquake of April 4, 2010." *Proc. of the 4th IASPEI/IAEE International Symposium*, 23-26.

Kohler, M. D., Filippitzis, F., Heaton, T. H., Clayton, R. W., Guy, R. G., Bunn, J. J., and Chandy, K. M. (2020). "2019 Ridgecrest earthquake reveals areas of Los Angeles that amplify shaking of high-rises." *Seis. Res. Lett*., 91(6), 3370–3380, doi:10.1785/0220200170.

Kohler, M. D., Massari, A., Heaton, T. H., Kanamori, H., Hauksson, E., Guy, R., Clayton, R. W., Bunn, J., and Chandy, K. M. (2016). "Downtown Los Angeles 52-story high-rise and free-field response to an oil refinery explosion." *Earthquake Spectra*, 32(3), 1793-1820. doi:10.1193/062315EQS101M.

Lee, E. J. et al. (2014). "Full-3-D tomography for crustal structure in southern California based on the scattering-integral and the adjoint-wavefield methods." *J. Geophys. Res.*, 119(8), 6421-6451.

Los Angeles Times (2020). "L.A. signs off on $1-billion 'mini-city' in the west San Fernando Valley." by David Zahniser, December 2, 2020. https://www.latimes.com/california/story/2020-12-02/l-a-san-fernando-valley-warner-center-mini-city.

Ponti, D., and Martin, P. P. (2021). "Development of a chronostratigraphic hydrogeologic framework model." In *Development of a groundwater-simulation model in the Los Angeles Coastal Plain, Los Angeles County, California*. S. R. Paulinski (ed.). *U.S.G.S.*

Scientific Investigations Report 2021-XXXX, X p., https://doi.org/10.31333/sir2021xxxx (in press).

Shaw, J., Plesch, A., Tape, C., Suess, M. P., Jordan, T. H., Ely, G. Hauksson, E., Tromp, J., Tanimoto, T., Graves, R., Olsen, K., Nicholson, C., Maechling, P. J., Rivero, C., Lovely, P., Brankman, C. M., and Munster, J. (2015). "Unified Structural Representation of the southern California crust and upper mantle." *Earth Plan. Sci. Lett*., 415, 1–15, doi:10.1016/j.epsl.2015.01.016.

Taranath, B. S. (1997). *Steel, Concrete, and Composite Design of Tall Buildings*. 2nd edition, McGraw-Hill, San Francisco.

Thompson, E. (2018). "An updated Vs30 map for California with geologic and topographic constraints." U.S. Geological Survey data release, doi:10.5066/F7JQ108S.

Wald, D., and Graves, R. (1998). "The seismic response of the Los Angeles basin, California." *Bull. Seis. Soc. Am*., 88(2), 337-356.

Wills, C. J., Gutierrez, C. I., Perez, F. G., and Branum, D. M. (2015). "A Next Generation V S 30 Map for California Based on Geology and Topography." *Bull. Seis. Soc. Am*., 105(6), 3083-3091, doi:10.1785/0120150105.